Journal of Power Sources 196 (2011) 2387–2392

Contents lists available at ScienceDirect

Journal of Power Sources

journal homepage: www.elsevier.com/locate/jpowsour

Microwave-assisted hydrothermal synthesis of crystalline WO_3–$WO_3 \cdot 0.5H_2O$ mixtures for pseudocapacitors of the asymmetric type

Kuo-Hsin Chang[a,b], Chi-Chang Hu[a,*], Chao-Ming Huang[a], Ya-Ling Liu[a], Chih-I Chang[a]

[a] Department of Chemical Engineering, National Tsing Hua University, 101, Section 2, Kuang Fu Road, Hsin-Chu 30013, Taiwan
[b] Department of Chemical Engineering, National Chung Cheng University, Chia-Yi 621, Taiwan

ARTICLE INFO

Article history:
Received 22 July 2010
Received in revised form
23 September 2010
Accepted 24 September 2010
Available online 1 October 2010

Keywords:
Tungsten oxide
Microwave-assisted hydrothermal synthesis
Electrochemical capacitor
Asymmetric type

ABSTRACT

Crystalline tungsten oxide mixtures, WO_3–$WO_3 \cdot 0.5H_2O$, prepared by microwave-assisted hydrothermal (MAH) synthesis at 180 °C for various periods, show capacitive-like behavior at 200 mV s^{-1} and $C_S \approx 290$ F g^{-1} at 25 mV s^{-1} in 0.5 M H_2SO_4 between −0.6 and 0.2 V. Oxide rods can be obtained via the MAH process even when the synthesis time is only 0.75 h while $WO_3 \cdot 0.5H_2O$ sheets with poor capacitive performances are obtained by a normal hydrothermal synthesis process at the same temperature for 24 h. The aspect ratio of tungsten oxide rods is found to increase with prolonging the MAH time while all oxides consist of WO_3 and $WO_3 \cdot 0.5H_2O$. The oxide mixtures prepared by the MAH method with annealing in air at temperatures ≤400 °C show promising performances for electrochemical capacitors (ECs). Due to the narrow working potential window of the oxide mixtures, an aqueous EC of the asymmetric type, consisting of a WO_3–$WO_3 \cdot 0.5H_2O$ anode and a $RuO_2 \cdot xH_2O$ cathode, with a potential window of 1.6 V is demonstrated in this work, which shows the device energy and power densities of 23.4 W kg^{-1} and 5.2 kW kg^{-1}, respectively.

1. Introduction

Electrochemical capacitors (ECs) have been proposed to bridge the critical performance gap between the conventional capacitors of high power densities and the batteries/fuel cells of high energy densities because their unique characteristics cover a broad region on the power vs. energy density plane [1,2]. This type of power-oriented devices with high energy efficiencies and long cycle life [3–5] have been used as the assistant and buffering systems for several primary power sources (e.g., electric vehicles, hybrid electric vehicles, and many typical stop-and-go systems) and renewable energy generation systems (wind-power systems and solar cells). Accordingly, ECs, offering transient but extremely high powers for time-dependent power needs of modern electronics and power systems, have been considered as one of the most important next generation energy storage devices [1–5].

Based on the charge storage mechanism, ECs can be generally divided into three categories. The electrode materials of electrical double-layer capacitors (EDLCs) are generally highly porous materials with high specific surface area, such as activated carbons, because electricity stored within the materials is proportional to the electrolyte-accessible surface area [6]. On the other hand, pseudocapacitors generally show very high specific capacitance because they employ the electrochemically active materials with highly reversible, superficial redox reactions [7,8]. Transition metal oxides, such as crystalline hydrous ruthenium dioxide (denoted as $RuO_2 \cdot xH_2O$) [9,10], are such a class of materials that have drawn extensive and intensive research attention in recent years. The third type is the so-called hybrid-type asymmetric ECs usually consisting of an EDLC electrode and a pseudocapacitive one [11,12], while asymmetric ECs with two pseudocapacitive electrodes have also been proposed [13–15].

Tungsten oxides in both crystalline and amorphous forms are widely studied as an electrode material for sensors and electrochromic devices [16,17]. Unfortunately, the electrochemical properties of both amorphous and crystalline WO_3 are not suitable for the application of ECs because of the limited potential window as well as the relatively poor reversibility of proton and Li-ion intercalation/de-intercalation [18,19]. However, Takasu et al. in 1999 proposed a oxide composite consisting of Ti, V, and W oxides for the application of ECs [20] meanwhile Jeong and Manthiram reported that RuO_2 coated with WO_3 showed good capacitive performances in both acidic and alkaline media in 2001 [21]. Recently, amorphous tungsten oxide with microwave radiation was reported to be a promising electrode material for ECs [22]. Accordingly, tungsten oxides of certain microstructures should be of pseudocapacitive behavior. Since the potential window for the reversible intercalation/de-intercalation of protons within tungsten oxides

* Corresponding author. Tel.: +886 3 573 6027; fax: +886 3 5756027.
E-mail address: cchu@che.nthu.edu.tw (C.-C. Hu).

0378-7753/$ – see front matter © 2010 Elsevier B.V. All rights reserved.
doi:10.1016/j.jpowsour.2010.09.078

is in the UPD (underpotential deposition) and OPD (overpotential deposition) hydrogen regions [23] meanwhile concentrated acidic solutions are suitable electrolytes for the redox transitions of tungsten oxides [23,24], a tungsten oxide anode and a RuO_2 cathode is proposed to construct an asymmetric EC with a wide working voltage to advance the energy density of ECs in this work.

Many chemical routes, such as hydrothermal synthesis [25], precipitation method [26], and electrochemical deposition [27] were developed to prepare tungsten oxides. However, tungsten oxides in both crystalline and amorphous forms prepared by these methods generally show unacceptable performances for the EC application. Accordingly, microwave irradiation is considered as a promising method [22]. Here, a novel method, microwave-assisted hydrothermal (MAH) process, is proposed to synthesize tungsten oxides with high-rate capability for ECs. The textural and electrochemical characteristics were investigated in this work. Finally, an asymmetric EC, consisting of a tungsten oxide anode and a RuO_2 cathode, with a working voltage of 1.6 V is demonstrated in this work.

2. Experimental

Tungsten oxides were synthesized through a MAH process from a solution containing 0.1 M $Na_2WO_4{\cdot}2H_2O$ and 1.0 M NaCl with pH = 2.0 adjusted by 4 M H_2SO_4. This solution was heated from room temperature to 180 °C and kept at this temperature with an air-flow cooling for 0.75–3 h at a constant power of 200 W in a microwave reactor (Discover, CEM), and then, cooled to room temperature with the same air-flow. The oxides were obtained by means of a centrifuge and washed with de-ionized water several times. Some oxides before coating were annealed in air at various temperatures for 2 h. For a comparison purpose, a tungsten oxide was synthesized through a normal hydrothermal process from the same solution at 180 °C in an oven for 24 h.

The pretreatment procedure of 10 mm × 10 mm × 3 mm graphite substrates (Nippon Carbon EG-NPL, N.C.K.) completely followed our previous work [10]. Tungsten oxide was drop-coated onto the pretreated graphite electrode by a pipette with water vaporized at ca. 80 °C. Repeat the procedure several times until the mass of a dried tungsten oxide coating film is equal to ca. 2.0 mg cm^{-2}. This electrode was kept in a vacuum oven at 80 °C overnight. These dried electrodes were carefully coated with polytetrafluorene ethylene films with an exposed surface area of 1 cm^2 for electrochemical characterisation.

The crystalline structures of samples were characterized by an X-ray powder diffractometer (CuKα, Ultima IV, Rigaku). The powder samples were measured at a scan rate of 2° min^{-1}. Morphologies of samples were examined by a field emission scanning electron microscope (FE-SEM, Hitachi S4800 type I).

Electrochemical characteristics were obtained by an electrochemical analyzer system, CHI 633A (CH Instruments, USA) in a three-compartment cell. An Ag/AgCl electrode was used as the reference and a piece of platinum gauze was employed as the counter electrode. A Luggin capillary was used to minimize errors due to *iR* drop in the electrolyte. For the two-electrode test, CVs were also measured by the same instrument meanwhile the working electrode is tungsten oxide while the counter and reference electrodes were connected to a $RuO_2{\cdot}xH_2O$-coated Ti electrode. All solutions used in this work were prepared with 18 MΩ cm de-ionized water produced by a reagent water system (Milli-Q SP, Japan).

3. Results and discussion

Fig. 1 shows the XRD patterns of tungsten oxides prepared by the MAH method for different reaction times meanwhile the result of an oxide prepared through a normal hydrothermal process for 24 h is also given for comparison purposes. On curve 1, this pattern can be mainly attributed to the tungsten trioxide of the hydrous form, $WO_3{\cdot}0.5H_2O$ (PDF#44-0363). Based on the diffraction peak of face (1 1 1) and Scherrer equation [28], the average crystal size of this oxide is ca. 9.9 nm, indicating that $WO_3{\cdot}0.5H_2O$ nanocrystallites can be effectively formed via a normal hydrothermal mode. On curve 2, the XRD pattern shows the presence of two crystalline phases, WO_3 (PDF#33-1387) and $WO_3{\cdot}0.5H_2O$. The average sizes of WO_3 (based on the diffraction peak of face (2 0 0)) and $WO_3{\cdot}0.5H_2O$ crystallites are equal to 16.8 and 14.8 nm, respectively. The above difference is attributable to the more efficient excitation of W ions and water molecules in the reaction medium through the microwave heating [22]. From an examination of patterns 2–5 in Fig. 1, all samples prepared by means of the MAH process can be considered as a mixture consisting of WO_3 and $WO_3{\cdot}0.5H_2O$ crystallites. The diffraction intensities corresponding to WO_3 and $WO_3{\cdot}0.5H_2O$ crystallites respectively increase and decrease with prolonging the MAH time, suggesting that WO_3 is easily formed via the MAH process.

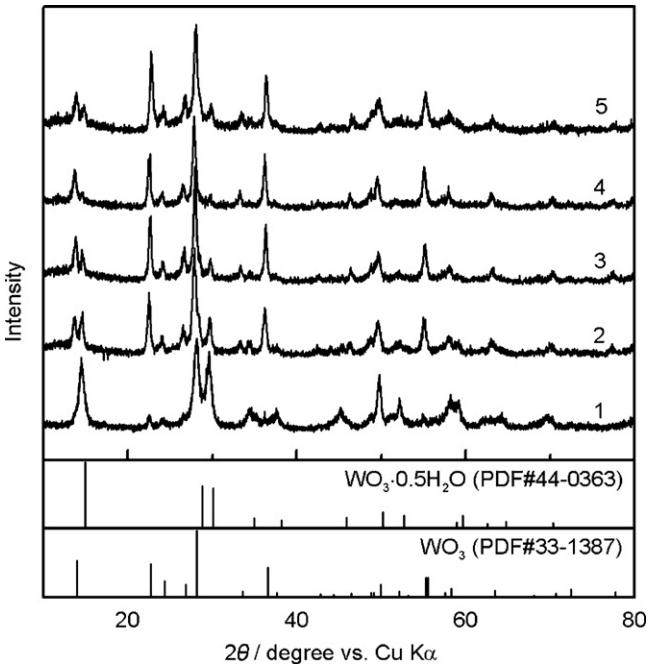

Fig. 1. XRD patterns of tungsten oxide prepared (1) by normal hydrothermal synthesis at 180 °C for 24 h and via the MAH process at 180 °C for (2) 0.75 h, (3) 1.5 h, (4) 2 h, and (5) 3 h.

The morphologies of tungsten oxides are also examined in this work, which are shown in Fig. 2. From Fig. 2A and B, $WO_3{\cdot}0.5H_2O$ generally shows the stacks of oxide sheets although some rod-like powders are visible. In Fig. 2C and D, the mixture of WO_3 and $WO_3{\cdot}0.5H_2O$ crystallites can be considered as aggregates of short rods with their diameter <50 nm. The rod morphology of this mixture becomes wire-like by prolonging the MAH time from a comparison of Fig. 2E–J, attributable to better crystalline quality of both oxides from the XRD patterns in Fig. 1. In addition, every wire can be considered as a bundle of fine wires although aggregates of short rods are still clearly visible in these samples. These oxide wires favorably make a three-dimensional porous network architecture, which is good for electrolyte penetration into the whole oxide matrix, favorable to the electrochemical energy storage systems of the high-power applications (e.g., ECs).

The electrochemical characteristics of all tungsten oxides prepared in this work were examined by cyclic voltammetry in 0.5 M H_2SO_4 and the typical results are shown in Fig. 3. On curve

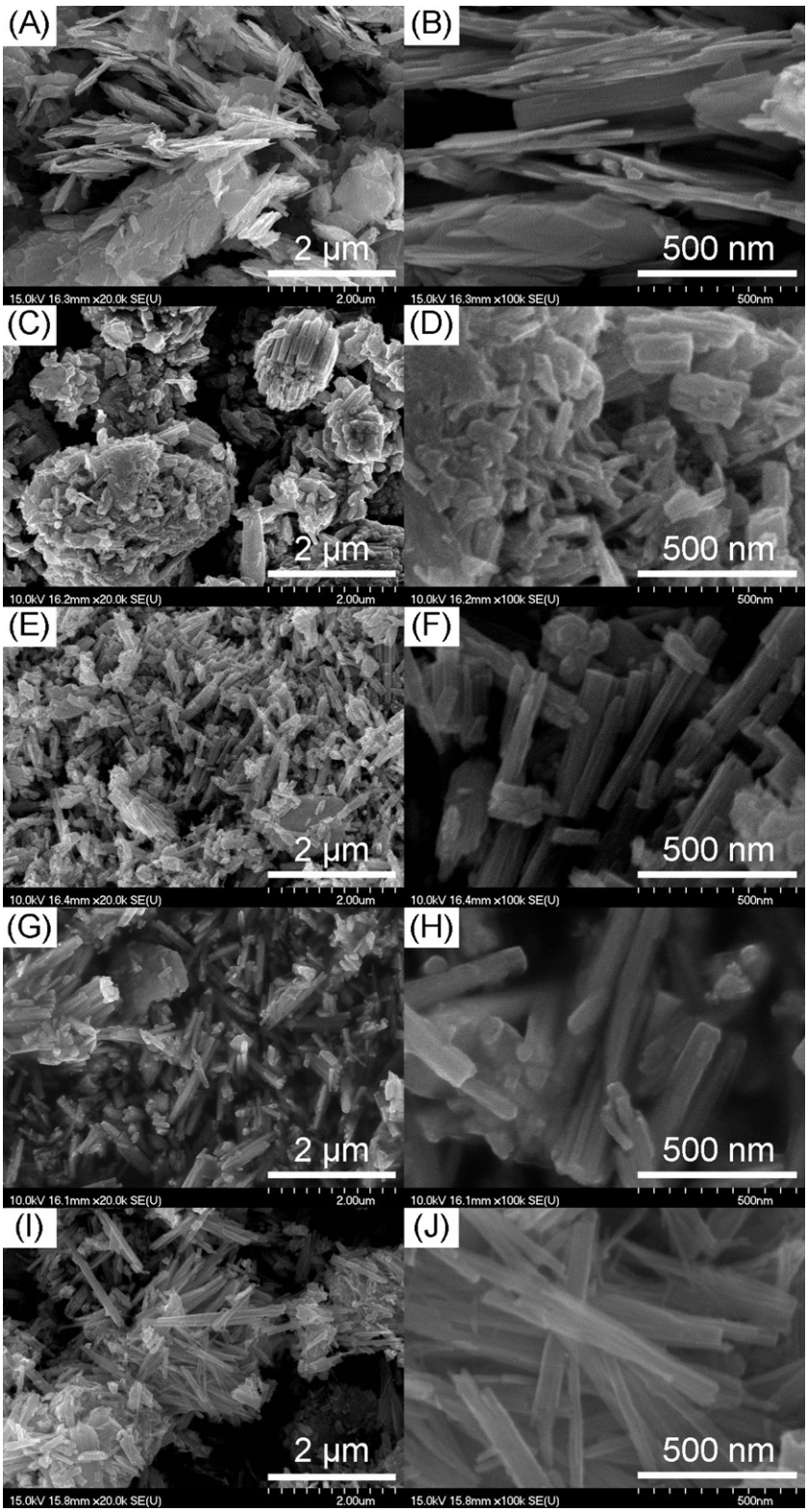

Fig. 2. SEM images of tungsten oxide prepared (A, B) by normal hydrothermal synthesis at 180 °C for 24 h and (C–J) via the MAH process at 180 °C for (C, D) 0.75 h, (E, F) 1.5 h, (G, H) 2 h, and (I, J) 3 h.

1, there is a pair of broad redox peaks in the potential region from −0.3 to −0.6 V, corresponding to the proton intercalation/de-intercalation within $WO_3{\cdot}0.5H_2O$. The electrochemical reversibility is fair but the charges stored in this material are generally low. On curve 2, the charges stored in this WO_3–$WO_3{\cdot}0.5H_2O$ mixture is much higher than that in $WO_3{\cdot}0.5H_2O$ (see curve 1). The i–E curve on the positive sweep is generally symmetric to that on the negative sweep, revealing the capacitive behavior although an additional pair of redox peaks is found between 0.2 and −0.1 V. Accordingly, the electrochemical reversibility of proton intercalation/de-intercalation in this mixture is better than that in $WO_3{\cdot}0.5H_2O$ synthesized by the normal hydrothermal process.

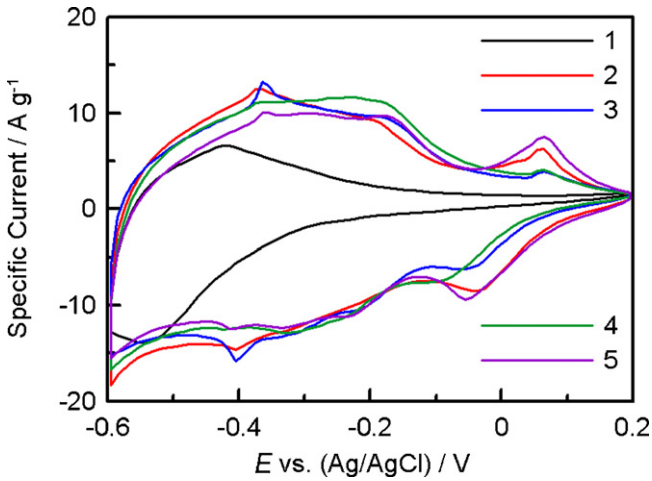

Fig. 3. Cyclic voltammograms of tungsten oxide prepared (1) by a normal hydrothermal synthesis process at 180 °C for 24 h and via the MAH process at 180 °C for (2) 0.75 h, (3) 1.5 h, (4) 2 h, and (5) 3 h. CVs were measured at 25 mV s^{-1} in 0.5 M H_2SO_4 at 25 °C.

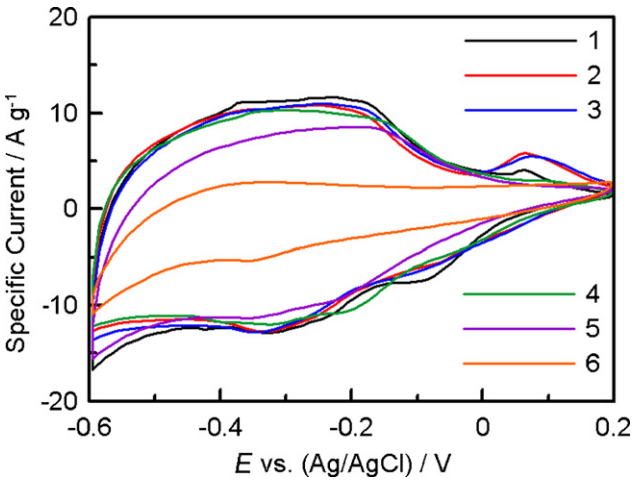

Fig. 4. Cyclic voltammograms of tungsten oxide prepared by microwave-assisted hydrothermal synthesis at 180 °C for 2 h with annealing in air at (1) as-prepared, (2) 150 °C, (3) 200 °C, (4) 300 °C, (5) 400 °C, and (6) 500 °C for 2 h. CVs were measured at 25 mV s^{-1} in 0.5 M H_2SO_4 at 25 °C.

From a comparison of curves 2–5, the oxide mixtures show very similar i–E responses, indicating their promising properties for the pseudo-capacitor application. On the other hand, from the symmetry of CV curves, the WO_3–$WO_3{\cdot}0.5H_2O$ mixture with MAH time equal to 2 h is considered to be the most suitable electrode material for ECs although the specific capacitance of all MAH-derived tungsten oxides is approximately the same (ranging from 280 to 300 F g^{-1}).

Annealing in air may change the microstructure of tungsten oxides, leading to improvements in the electrochemical properties and stability [29]. Fig. 4 shows the cyclic voltammograms of tungsten oxide with the MAH time equal to 2 h and annealing in air for 2 h at different temperatures. From a comparison of all CV curves, no obvious change is found when the annealing temperature is ≤300 °C, while an obvious decrease in the voltammetric charge is found with a further rise in the annealing temperature. The order of annealing tem-

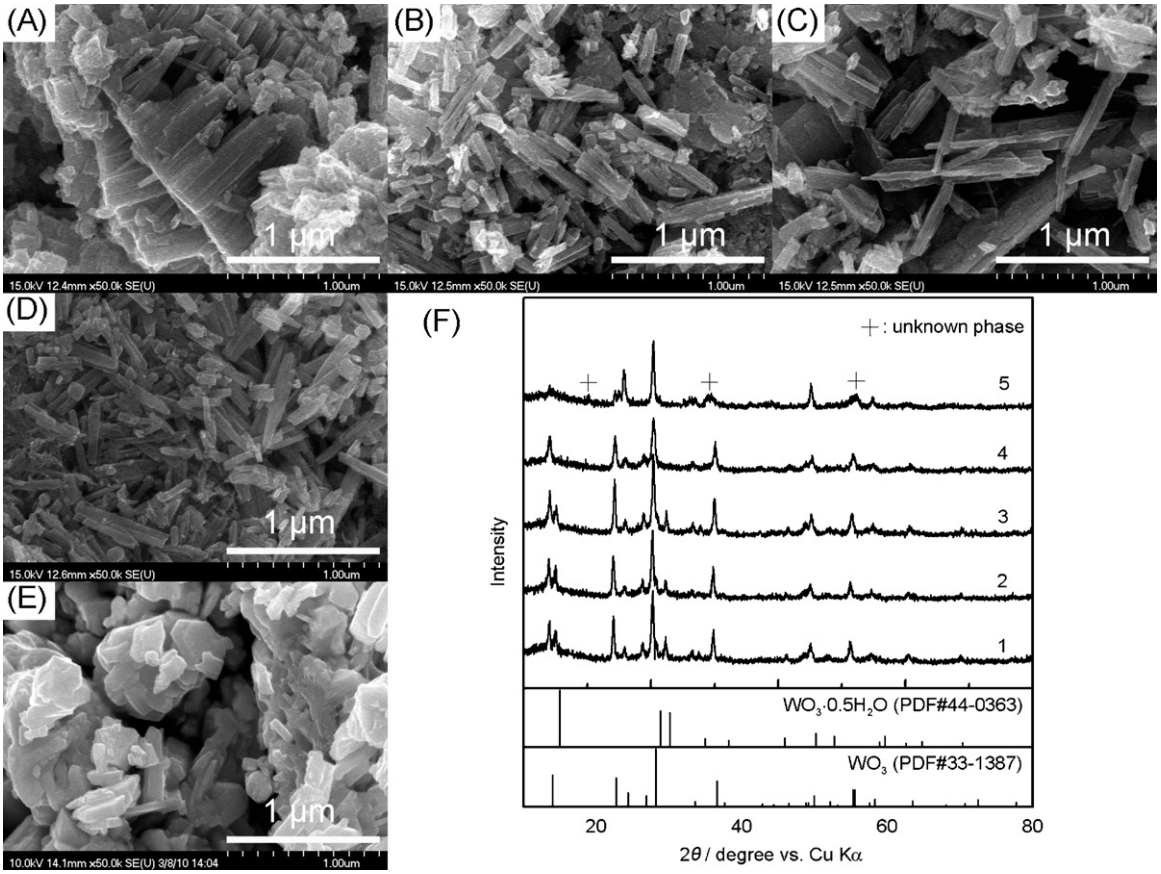

Fig. 5. (A–E) SEM images and (F) XRD patterns of tungsten oxide prepared by microwave-assisted hydrothermal synthesis at 180 °C for 2 h with annealing in air at (A,1) 150 °C, (B,2) 200 °C, (C,3) 300 °C, (D,4) 400 °C, and (E,5) 500 °C for 2 h.

perature with respect to decreasing the specific capacitance is: as-prepared (293 F g^{-1}) ≈ 150 °C (277 F g^{-1}) ≈ 200 °C (287 F g^{-1}) ~300 °C (251 F g^{-1}) > 400 °C (210 F g^{-1}) ≫ 500 °C (93 F g^{-1}). The above change in electrochemical properties should result from a phase transformation or microstructure variation of the WO_3–WO_3·0.5H_2O mixture annealed at temperatures ≥400 °C.

Fig. 5A–E shows the SEM images of the WO_3–WO_3·0.5H_2O mixture prepared by MAH synthesis at 180 °C for 2 h with annealing in air at various temperatures. In general, the morphology of this mixture is not significantly changed by annealing when the temperatures are ≤300 °C, while significant sintering of tungsten oxide is found at annealing temperatures ≥400 °C. The above results are generally consistent with the CV results shown in Fig. 4. This inference is supported by the XRD patterns shown in Fig. 5F where an unknown phase is found on curve 5 although WO_3 crystallites are still visible. The significant decease in the crystal size of resultant WO_3 at temperatures ≥500 °C also indicates the collapses of WO_3 and WO_3·0.5H_2O crystals. Based on the above electrochemical and textural characteristics, the WO_3–WO_3·0.5H_2O mixture annealed in air between 200 and 300 °C for 2 h is considered as the most suitable electrode material for ECs.

To demonstrate the excellent performances of annealed WO_3–WO_3·0.5H_2O mixtures, Fig. 6A shows the typical cyclic voltammograms measured at different scan rates for this oxide mixture annealed in air at 300 °C for 2 h. Clearly, this oxide shows good capacitive behavior at 250 mV s^{-1} although certain distortion in the i–E curves is found with increasing the scan rate. The above result suggests the good power capability of this annealed oxide. This statement is supported by the results that the capacitive current density is quasi-linearly proportional to the scan rate of CV (see Fig. 6B) and that about 66% capacitance retention is obtained when the scan rate is changed from 25 to 200 mV s^{-1} (see Fig. 6C). Consequently, the WO_3–WO_3·0.5H_2O mixture annealed in air at 300 °C for 2 h is considered as the most suitable electrode material for ECs.

Note that tungsten oxide is a proton intercalation/de-intercalation material and its activation overpotential for the hydrogen evolution reaction is fairly high (supported by the CV curves in Fig. 4). Hence, the WO_3–WO_3·0.5H_2O mixture prepared in this work is suitable for the anode of ECs in the asymmetric type because of its narrow working potential window, from −0.6 to ca. 0 V, for the proton intercalation/de-intercalation. Since RuO_2·xH_2O nanocrystallites shows excellent capacitive performances between 0 and 1.0 V in aqueous acid media [9,10], an asymmetric EC consisting of the WO_3–WO_3·0.5H_2O anode and a RuO_2·xH_2O cathode should show a working voltage of 1.6 V to enhance the energy density of this device ($E = CV^2/2$ where E, C, and V indicate the energy, capacitance, and working voltage of ECs) [1,12]. Fig. 7A shows the cyclic voltammograms of a RuO_2·xH_2O cathode and a WO_3–WO_3·0.5H_2O anode in 0.5 M H_2SO_4. Clearly, the working potential regions of RuO_2·xH_2O and WO_3–WO_3·0.5H_2O are complementary and their charges stored in their respective CVs can be adjusted to be equal by controlling the mass of active materials. Fig. 7B shows the typical cyclic voltammograms of a supercapacitor of the asymmetric type consisting of the above two electrodes in 0.5 M H_2SO_4. Clearly, this EC shows good capacitive performances at different scan rates. Moreover, the plots of specific energy vs. specific power for both symmetric (RuO_2–RuO_2) and asymmetric (WO_3–RuO_2) capacitors are shown in Fig. 7C to demonstrate the benefits of asymmetric capacitors. Clearly, the specific energy and specific power of asymmetric capacitor are significantly enhanced because of its wider cell voltage in comparing with the symmetric type although the specific capacitance of RuO_2·xH_2O nanocrystallites used here is much higher than that of WO_3–WO_3·0.5H_2O. Based on the total mass of all active materials on the cathode and anode (ca. 4 mg cm^{-2}), the energy and power densities of this device are respectively equal to 23.4 W kg^{-1} and 5.2 kW kg^{-1}, when the scan rate is equal to 100 mV s^{-1}, which is promising in the application of next generation ECs.

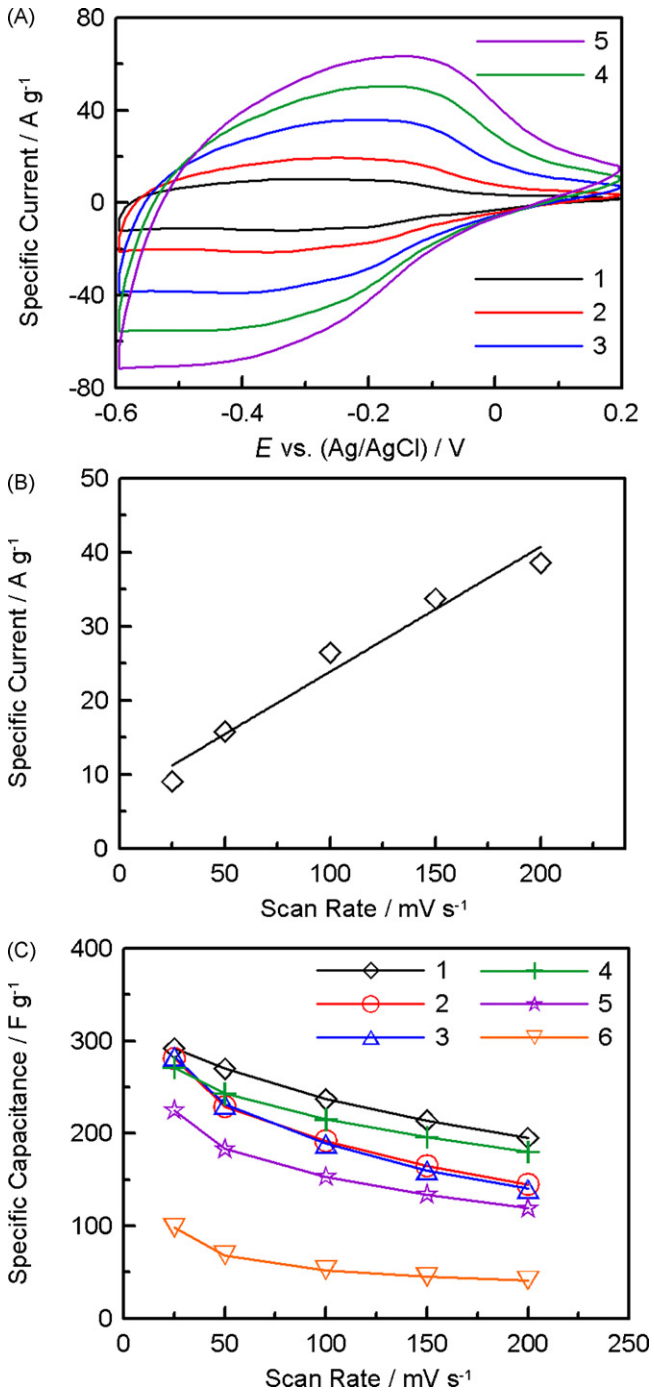

Fig. 6. (A) Cyclic voltammograms of tungsten oxide prepared by microwave-assisted hydrothermal synthesis at 180 °C for 2 h with annealing in air at 300 °C for 2 h. CVs were measured at (1) 25 mV s^{-1}, (2) 50 mV s^{-1}, (3) 100 mV s^{-1}, (4) 150 mV s^{-1}, and (5) 200 mV s^{-1} and dependence of (B) current density at −0.4 V and (C) C_S on the scan rate of CV for tungsten oxide prepared by microwave-assisted hydrothermal synthesis at 180 °C for 2 h with annealing in air at (1) as-prepared, (2) 150 °C, (3) 200 °C, (4) 300 °C, (5) 400 °C, and (6) 500 °C for 2 h.

Unfortunately, the cycle life of as-prepared WO_3–WO_3·0.5H_2O is poor since about 28% capacitance loss was found when 100 cycles of CV between 0.2 and −0.6 V were applied. Accordingly, a systematical investigation, including changing synthesis parameters such as MAH temperature, MAH reaction time, and pH, anions, cations, concentration, etc. in the precursor solutions, varying the anneal-

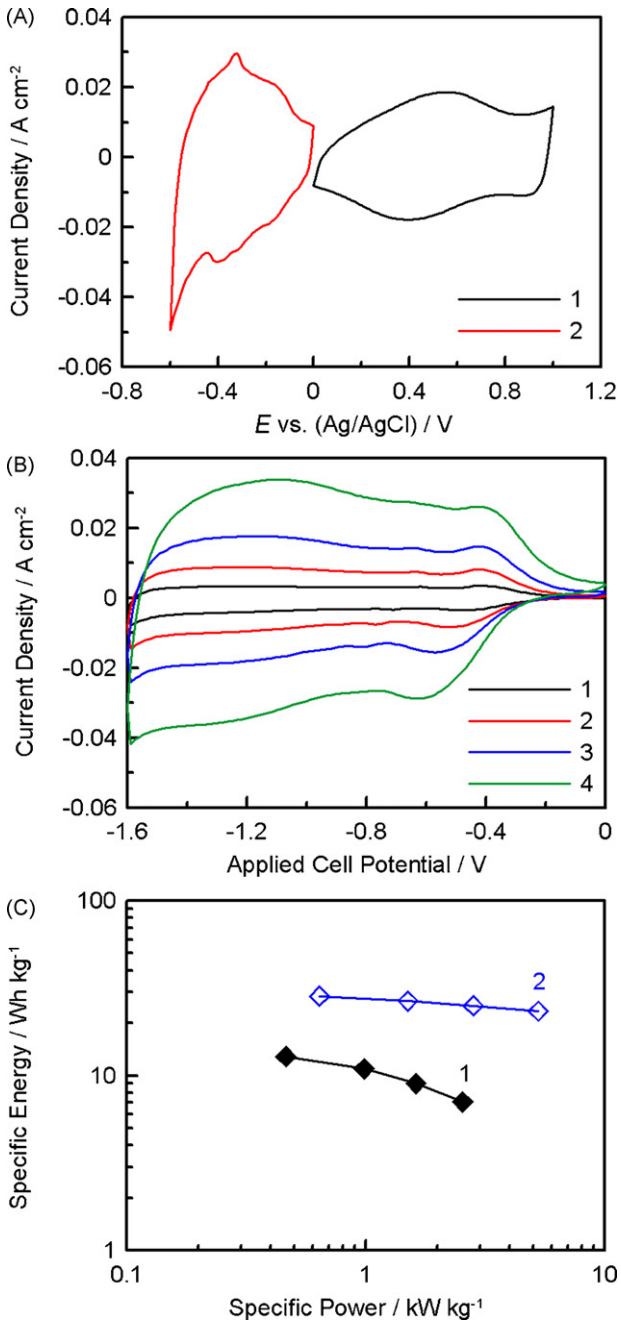

Fig. 7. (A) Cyclic voltammograms of (1) $RuO_2{\cdot}xH_2O$ and (2) tungsten oxide measured at 25 mV s^{-1} in 0.5 M H_2SO_4; (B) cyclic voltammograms of a supercapacitor of the asymmetric type consisting of a tungsten oxide anode and a $RuO_2{\cdot}xH_2O$ cathode measured at (1) 10 mV s^{-1}, (2) 25 mV s^{-1}, (3) 50 mV s^{-1}, and (4) 100 mV s^{-1} in 0.5 M H_2SO_4; (C) The plots of specific energy vs. specific power for (1) symmetric (RuO_2–RuO_2) and (2) asymmetric (RuO_2–WO_3) capacitors. Here the total weight of all active materials (including cathode and anode) for both symmetric and asymmetric capacitors is equal to ca. 4 mg cm^{-2}.

ing conditions (e.g., temperatures, duration, atmospheres, etc.), and modifying the life-test environments (e.g., potential region, pH and additives in electrolytes, supporting electrolyte, etc.), on improving the cycle life of WO_3–$WO_3{\cdot}0.5H_2O$ is ongoing.

4. Conclusions

Crystalline tungsten oxide mixtures, WO_3–$WO_3{\cdot}0.5H_2O$, were prepared by microwave-assisted hydrothermal (MAH) synthesis at 180 °C for various periods, which showed capacitive-like behavior at 200 mV s^{-1} and $C_S \approx 290$ F g^{-1} at 25 mV s^{-1} in 0.5 M H_2SO_4 between −0.6 and 0.2 V. Oxide rods can be obtained via the MAH process even when the synthesis time is only 0.75 h while $WO_3{\cdot}0.5H_2O$ sheets with poor capacitive performances were obtained by a normal hydrothermal synthesis process at the same temperature for 24 h. The aspect ratio of tungsten oxide rods was found to increase with prolonging the MAH time while all oxides consist of WO_3 and $WO_3{\cdot}0.5H_2O$. The oxide mixtures prepared by the MAH method with annealing in air at temperatures ≤400 °C show promising performances for electrochemical capacitors (ECs). Due to the narrow working potential window of the oxide mixtures, an aqueous EC of the asymmetric type, consisting of a WO_3–$WO_3{\cdot}0.5H_2O$ anode and a $RuO_2{\cdot}xH_2O$ cathode, with a potential window of 1.6 V is demonstrated in this work, which shows the device energy and power densities of ca. 23.4 W kg^{-1} and 5.2 kW kg^{-1}, respectively.

Acknowledgments

The financial support of this work, by the National Science Council of the ROC Taiwan under contract no. NSC 98-3114-E-007-011 and the boost program of National Tsing Hua University, is gratefully acknowledged.

References

[1] B.E. Conway, Electrochemical Supercapacitors, Kluwer–Plenum Pub. Co., New York, 1999.
[2] R. Kotz, M. Carlen, Electrochim. Acta 45 (2000) 2483.
[3] A. Burke, J. Power Sources 91 (2000) 37.
[4] M. Winter, R.J. Brodd, Chem. Rev. 104 (2004) 4245.
[5] J.R. Miller, A.F. Burke, Interface 17 (2008) 53.
[6] E. Frackowiak, F. Beguin, Carbon 39 (2001) 937.
[7] S. Hadzi-Jordanov, H. Angerstein-Kozlowska, M. Vukovic, B.E. Conway, J. Electrochem. Soc. 125 (1978) 1471.
[8] D. Choi, G.E. Blomgren, P.N. Kumta, Adv. Mater. 18 (2006) 1178.
[9] J.P. Zheng, P.J. Cygan, T.R. Jow, J. Electrochem. Soc. 142 (1995) 2699.
[10] C.C. Hu, W.C. Chen, K.H. Chang, J. Electrochem. Soc. 151 (2004) A281.
[11] T. Brousse, M. Toupin, D. Belanger, J. Electrochem. Soc. 151 (2004) A614.
[12] P.J. Hung, K.H. Chang, Y.F. Lee, C.C. Hu, K.M. Lin, Electrochim. Acta 55 (2010) 6015.
[13] S.B. Ma, K.W. Nam, W.S. Yoon, X.Q. Yang, K.Y. Ahn, K.H. Oh, K.B. Kim, Electrochem. Commun. 9 (2007) 2807.
[14] K. Naoi, P. Simon, Interface 17 (2008) 34.
[15] K.C. Ng, S. Zhang, C. Peng, G.Z. Chen, J. Electrochem. Soc. 156 (2009) A846.
[16] I. Jimenez, J. Arbiol, G. Dezanneau, A. Cornet, J.R. Morante, Sens. Actuators B: Chem. 93 (2003) 475.
[17] J. Livage, D. Ganguli, Sol. Energy Mater. Sol. Cells 68 (2001) 365.
[18] C.G. Granqvist, Sol. Energy Mater. Sol. Cells 60 (2000) 201.
[19] D.J. Kim, S.I. Pyun, Y.M. Choi, Solid State Ionics 109 (1998) 81.
[20] Y. Takasu, S. Mizutani, M. Kumagai, S. Sawaguchi, Y. Murakami, Electrochem. Sol. State Lett. 2 (1999) 1.
[21] Y.U. Jeong, A. Manthiram, J. Electrochem. Soc. 148 (2001) A189.
[22] C.C. Huang, W. Xing, S.P. Zhou, Scr. Mater. 61 (2009) 985.
[23] D.J. Kim, S.I. Pyun, Electrochim. Acta 43 (1998) 2341.
[24] J. Wang, E. Khoo, P.S. Lee, J. Ma, J. Phys. Chem. C 113 (2009) 9655.
[25] X.L. Li, J.F. Liu, Y.D. Li, Inorg. Chem. 42 (2003) 921.
[26] O. Nimittrakoolchai, S. Supothina, J. Mater. Chem. Phys. 112 (2008) 270.
[27] P.M.S. Monk, S.L. Chester, Electrochim. Acta 38 (1993) 1521.
[28] B.D. Cullity, Elements of X-ray Diffraction, 2nd ed., Addison-Wesley, Reading, MA, 1978.
[29] S.Y. Park, J.M. Lee, C. Noh, S.U. Son, J. Mater. Chem. 19 (2009) 7959.